





Padded Coprime Arrays for Improved DOA Estimation: Exploiting Hole Representation and Filling Strategies

Wang Zheng , Xiaofei Zhang , Yunfei Wang , Jinqing Shen, and Benoit Champagne , *Senior Member, IEEE*

Abstract—As a generalized coprime array structure, the coprime array with displaced subarrays (CADiS) allows a large minimum inter-element spacing by introducing a specific displacement between two sparse subarrays. While this structure can effectively reduce mutual coupling, the holes in its difference co-array greatly decrease the achievable number of uniform degrees of freedom (DOFs). In this paper, we first provide a complete characterization for the hole locations in the difference co-array generated by a tailored CADiS (tCADiS) as the union of four subsets of locations related via simple symmetry properties. We then introduce two representation approaches for the hole locations, revealing that the latter can be generated from the differences between sensor locations in the subarray of tCADiS and a small uniform linear array, referred to as a padded subarray. Subsequently, we propose novel padded coprime arrays (PCAs) by incorporating the padded subarray into tCADiS to enlarge the consecutive segments in the difference co-array. This not only contributes to increase the number of available uniform DOFs, but also helps mitigating the mutual coupling by limiting the number of sensor pairs with small separations. Finally, numerical simulation results are provided to demonstrate the superiority of PCAs over existing sparse array configurations in terms of DOF, mutual coupling and DOA estimation accuracy.

Index Terms—Difference co-array, DOA estimation, mutual coupling, padded coprime arrays, uniform degrees of freedom.

Manuscript received March 13, 2020; revised June 22, 2020; accepted July 27, 2020. Date of publication July 31, 2020; date of current version August 20, 2020. This work was supported in part by China Scholarship Council 201806830081, in part by China NSF under Grants 61371169, 61631020, 61971217, 61971218, and 61601167, in part by Jiangsu NSF under Grant BK20161489, in part by the Open Research fund of State Key Laboratory of Millimeter Waves, Southeast University K201826, in part by the Fundamental Research Funds for the Central Universities under Grant NE2017103, in part by the postgraduate Research and Practice Innovation Program of Jiangsu Province KYCX18_0293, in part by the Fund of Sonar Technology Key Laboratory (Research on the theory and algorithm of signal processing for two-dimensional underwater acoustics coprime array), and in part by the Fund of Sonar Technology Key Laboratory (Range estimation and location technology of passive target via multiple array combination). The associate editor coordinating the review of this manuscript and approving it for publication was Prof. Remy Boyer. (*Corresponding author: Zhang Xiaofei.*)

Wang Zheng is with the College of Electronic and Information Engineering, Nanjing University of Aeronautics and Astronautics, Nanjing 210000, China, and is also with the Department of Electrical and Computer Engineering, McGill University, Montreal, QC H3A 0E9, Canada (e-mail: zwang@nuaa.edu.cn).

Xiaofei Zhang, Yunfei Wang, and Jinqing Shen are with the College of Electronic and Information Engineering, Nanjing University of Aeronautics and Astronautics, Nanjing 210000, China (e-mail: zhangxiaofei@nuaa.edu.cn; wyf9612@126.com; sjq_nuaa@163.com).

Benoit Champagne is with the Department of Electrical and Computer Engineering, McGill University, Montreal, QC H3A 0E9, Canada (e-mail: benoit.champagne@mcgill.ca).

Digital Object Identifier 10.1109/TSP.2020.3013389

I. INTRODUCTION

ARRAY signal processing, including adaptive beamforming and direction of arrival (DOA) estimation [1]–[6], has been extensively applied in various fields, such as astronomy, navigation, wireless communication and radar [7]–[10]. The conventional subspace-based DOA estimation algorithms, *e.g.*, MUSIC [4] and ESPRIT [5], can detect $T - 1$ sources at most with a T -sensor uniform linear array (ULA), which means that more antennas are required to identify an increased number of sources. Meanwhile, the spacing between adjacent sensors in a ULA is usually limited to $\lambda/2$ to circumvent spatial aliasing, where λ denotes the operating wavelength. This small spacing leads to severe mutual coupling which adversely impacts the DOA estimation.

Several methods [11]–[13] have been proposed to mitigate mutual coupling effects by utilizing more sophisticated models of antenna coupling. These methods attempt to estimate the mutual coupling coefficients, but unfortunately encounter deficiencies of model mismatch, reduced degrees of freedom (DOFs) and high computational cost. As an alternative approach, a sparse array configuration, namely the minimum redundancy array (MRA) [14], was proposed to enlarge the distance between adjacent sensors while offering large DOFs, as provided by the difference co-array. However, the sensor locations in the MRA are not available in closed-form and must therefore be calculated through a time-consuming search. In recent years, nested arrays (NA) [15] and coprime arrays [16], both with exact location expressions of the physical array and difference co-array, have aroused considerable attention. It was proved in [15], [16] that with these configurations, $O(T^2)$ DOFs can be achieved with only T antenna elements. While the NA configurations, including two-level NA [15], super NA (SNA) [17], [18] and augmented NA (ANA) [19], are sensitive to mutual coupling due to the densely assembled subarrays, the coprime arrays can tackle the problem with a sparser array structure.

An original co-prime array is obtained by interleaving two ULAs of length M and N , and inter-element spacing $\lambda N/2$ and $\lambda M/2$, respectively, where M and N are co-prime integers [16]. As an important improvement, the augmented coprime array (ACA) proposed in [20] can increase the length of consecutive segments in the difference co-array, termed here as consecutive co-array. Specifically, the length of the consecutive array is increased to $2MN + 2M - 1$ virtual sensors by adding an extra

M -sensor subarray ($M < N$) in the original coprime array structure. Different from the original coprime array and ACA with interleaved subarrays, the generalized coprime array [21] can enlarge the minimum spacing between sensors by splitting and translating the two interleaved subarrays composing the ACA. The resulting coprime array with displaced subarrays (CADiS) can drastically mitigate the mutual coupling. However, CADiS reduces the length of consecutive co-arrays, which in turn degrades the performance of DOA estimation algorithms based on spatial smoothing and Toeplitz matrix properties [15], [16], [22], [23], in addition to decreasing the number of uniform DOFs.

Some efforts have been made to enhance the consecutive co-array by designing extended coprime arrays. A thinned coprime array (TCA) was proposed in [24] to reduce the number of redundant physical sensors and simultaneously obtain the same number of uniform DOFs as ACA. In particular, few sensor pairs with small separations are involved in TCA and hence, this configuration can reduce mutual coupling. In [25], adopting the hole filling perspective, the authors proposed the coprime array with multi-period subarrays (CAMpS), but the complex analysis of the hole positions prevents the further improvements of the structure. A detailed investigation on the holes in the difference co-array of a newly constructed coprime array, namely the k -times extended coprime array (k ECA), was addressed in [26] from the viewpoint of hole identification and filling. In addition, a complementary coprime array (CCA) was proposed by filling the holes in the difference co-array of k ECA to obtain the hole-free property and hence an increase of uniform DOFs. Actually, the k ECA is an extension of ACA but extra sensor pairs with small separations still exist, which is the main cause of mutual coupling. Furthermore, since the complementary subarray is a compact array, CCA is much more sensitive to mutual coupling compared with k ECA.

In practical applications, the mutual coupling effect between the sensors with small separations cannot be neglected, that is, isotropic radiators without mutual coupling do not exist in reality. As a result, in this paper, we employ the more realistic received signal model by incorporating the widely-used expression of the mutual coupling coefficient [17]–[19], [27]–[30], which is inversely proportional to the separation between sensors. Specifically, we bring further improvements to the family of coprime array structure by considering two aspects: 1) lengthening the consecutive co-array by incorporating a padded subarray into CADiS, and 2) reducing mutual coupling by limiting the number of sensor pairs with small separations. In particular, we summarize our main contributions as follows.

- a) We provide a complete and concise characterization for the hole locations in the difference co-array generated by a tailored CADiS (tCADiS) as the union of four subsets of locations related via simple symmetry properties. This is in contrast to the work in [21] which only provides the location expression of the holes in the negative part of the cross-difference co-array.
- b) We introduce two representation approaches for the location of holes in the difference co-array generated by tCADiS and show that these locations can be obtained as

the differences between sensor locations in the subarray of tCADiS and a small ULA, termed as *padded subarray*. These representation approaches provide a basis for the extension of coprime array structures in our work.

- c) Based on the newly introduced representation approaches for hole locations, we propose two novel PCAs, named PCA-I and PCA-II, by incorporating the padded subarray into tCADiS to increase the number of uniform DOFs and limit the number of sensor pairs with small separations. Meanwhile, we introduce an extension for the PCA configuration and propose the extended PCA (ePCA), which is a sparser structure with more uniform DOFs compared to PCA-I and PCA-II. In addition, we solve the optimal PCAs for maximum uniform DOFs with a fixed number of sensors.
- d) We present and discuss extensive simulation results to demonstrate the merits of the proposed PCA configurations. It is noteworthy that the proposed PCAs mitigate the mutual coupling by reducing the sensor pairs with small separations as compared with existing ULA, nested arrays and coprime arrays.

The outline of this paper is given as follows. We provide the background and the motivation for our work in Section II. In Section III, we introduce two representation approaches for the hole locations and propose the PCAs. In Section IV, we compare the proposed PCAs with other existing sparse arrays in terms of DOF and mutual coupling. Numerical simulations are given in Sections V and VI concludes this paper.

Notations: We use upper-case (lower-case) bold characters to represent matrices (vectors). $(\cdot)^T$, $(\cdot)^*$ and $(\cdot)^H$, respectively, stand for the transpose, conjugation and conjugate transpose of a matrix or vector. $\text{diag}\{\mathbf{v}\}$ generates a diagonal matrix with the vector \mathbf{v} as its diagonal elements, while $\text{diag}\{\mathbf{V}\}$ takes the principal diagonal elements of matrix \mathbf{V} to construct a diagonal matrix. $\langle a_1, a_2 \rangle$ denotes an integer set $\{a \in \mathbb{Z} | a_1 \leq a \leq a_2\}$ and $\mathbb{Z} = \{0, \pm 1, \pm 2, \dots\}$. $\lfloor a \rfloor$ rounds a to the nearest integer with $\lfloor a \rfloor \leq a$ while $\lceil b \rceil$ rounds b to the nearest integer with $\lceil b \rceil \geq b$. $E\{\cdot\}$ is the expectation operator and $\min\{\cdot\}$ is the minimization operator. $\text{vec}(\mathbf{A})$ stands for the vectorization operator stacking the columns of a matrix \mathbf{A} . \otimes is the Kronecker product and \circ is the Khatri-Rao product. $\|\cdot\|_F$ denotes the Frobenius norm. $\text{Card}\{\cdot\}$ gives the cardinality. \mathbf{I}_n denotes an $n \times n$ identity matrix.

II. PRELIMINARIES

In this section, we first introduce some basic concepts and terminology in sparse array signal processing and then review the B -banded mutual coupling model. We then briefly review key results on hole locations in the difference co-array of CADiS [21] and address the motivation of this paper.

A. Sparse Array Signal Processing

Within a planar geometry, assume that K far-field narrowband signals with angles $\theta_k (k \in \langle 1, K \rangle)$ impinge on a T -element linear array with sensor locations given by the set $\mathbb{L} = \{d_t, t \in \langle 1, T \rangle\}$, where d_t denotes the distance of the t -th antenna from a

selected origin along the array axis, normalized by $\lambda/2$ where λ is the wavelength at the operating frequency. The received signal can be represented by

$$\mathbf{x}(l) = \mathbf{A}\mathbf{s}(l) + \mathbf{n}(l) \quad (1)$$

where $\mathbf{s}(l) = [s_1(l), s_2(l), \dots, s_K(l)]^T \in \mathbb{C}^{K \times 1}$ is the signal vector, $\mathbf{A} \in \mathbb{C}^{T \times K}$ is a directional matrix, $\mathbf{n}(l)$ is an additive noise term, $l \in \langle 1, L \rangle$ is the snapshot index, and L is the total number of snapshots. In this work, $\mathbf{n}(l)$ is modeled as a white Gaussian vector process with zero mean and covariance matrix $\sigma_n^2 \mathbf{I}_T$, where σ_n^2 is the element noise power. The signal vector is modeled as a temporally white zero-mean vector process with covariance matrix $\mathbf{R}_s = E\{\mathbf{s}(l)\mathbf{s}(l)^H\}$. Finally, the directional matrix takes the form $\mathbf{A} = [\mathbf{a}(\nu_1), \mathbf{a}(\nu_2), \dots, \mathbf{a}(\nu_K)] \in \mathbb{C}^{T \times K}$, where $\mathbf{a}(\nu)$ is the steering vector defined by [17].

$$\mathbf{a}(\nu_k) = [e^{-j\pi d_1 \nu_k}, e^{-j\pi d_2 \nu_k}, \dots, e^{-j\pi d_T \nu_k}]^T \quad (2)$$

where $\nu_k = \sin \theta_k$ and $k \in \langle 1, K \rangle$.

The covariance matrix of the received signal (1) is given by

$$\begin{aligned} \mathbf{R}_x &= E\{\mathbf{x}(l)\mathbf{x}(l)^H\} \\ &= \mathbf{A}\mathbf{R}_s\mathbf{A}^H + \sigma_n^2 \mathbf{I}_T \end{aligned} \quad (3)$$

In this sequel, we assume that the source signals are uncorrelated, *i.e.*, $\mathbf{R}_s = E\{\mathbf{s}(l)\mathbf{s}(l)^H\} = \text{diag}\{\sigma_1^2, \sigma_2^2, \dots, \sigma_K^2\}$, where σ_k^2 denotes the power of the k -th signal.

In sparse array signal processing, the difference co-array is usually generated from the physical array and then an augmented virtual array is utilized to offer increased number of DOFs.

Definition 1: For a physical array with location set \mathbb{L} , the difference co-array \mathbb{D} is defined as

$$\mathbb{D} = \{d_c | d_c = d_u - d_v; d_u, d_v \in \mathbb{L}\} \quad (4)$$

A consecutive co-array $\mathbb{U} \subseteq \mathbb{D}$ is defined as the uniform linear subarray of the difference co-array with maximum aperture [19] and it is noteworthy that a difference co-array can possess more than one consecutive co-array.

Definition 2: For a physical array, the total number of DOFs is defined as the cardinality of the difference co-array \mathbb{D} and the number of uniform DOFs is defined as the cardinality of the consecutive co-array \mathbb{U} [17].

To construct the equivalent received signal from the virtual array, we can vectorize \mathbf{R}_x as [15]

$$\begin{aligned} \mathbf{z} &= \text{vec}(\mathbf{R}_x) \\ &= (\mathbf{A}^* \circ \mathbf{A})\mathbf{p} + \sigma_n^2 \text{vec}(\mathbf{I}_T) \\ &= \mathbf{B}\mathbf{p} + \sigma_n^2 \text{vec}(\mathbf{I}_T) \end{aligned} \quad (5)$$

where $\mathbf{B} = [\mathbf{b}(\nu_1), \mathbf{b}(\nu_2), \dots, \mathbf{b}(\nu_K)]$, $\mathbf{b}(\nu_k) = \mathbf{a}^*(\nu_k) \otimes \mathbf{a}(\nu_k)$ and $\mathbf{p} = [\sigma_1^2, \sigma_2^2, \dots, \sigma_K^2]^T$. In particular, the entries of $\mathbf{b}(\nu_k)$ are arranged in the form of $e^{-j\pi(d_u - d_v)\nu_k}$ and hence the distinct rows in $\mathbf{b}(\nu_k)$ behave like the steering vectors of the difference co-array, where $d_u, d_v \in \mathbb{L}$. Furthermore, the equivalent received signals of the difference co-array and consecutive co-array can be extracted from \mathbf{z} . According to Section IV.A in [15], a spatially smoothed matrix can be calculated with \mathbf{z} and used to apply the ESPRIT algorithm, which is the same as the spatial smoothing ESPRIT (SS-ESPRIT)

in [19]. In practice, we estimate the covariance matrix \mathbf{R}_x with L snapshots, *i.e.*,

$$\hat{\mathbf{R}}_x = \frac{1}{L} \sum_{l=1}^L \mathbf{x}(l)\mathbf{x}(l)^H \quad (6)$$

B. Mutual Coupling

It is indicated in [27]–[30] that the mutual coupling coefficient c_d between two antenna elements is inversely related to their separation d , and that the mutual coupling matrix of a linear array can be modeled as a B -banded Toeplitz matrix [17], [19], [27]–[30]

$$[\mathbf{C}]_{p,q} = \begin{cases} 0 & |d_p - d_q| > B \\ c_{|d_p - d_q|} & |d_p - d_q| \leq B \end{cases} \quad (7)$$

where $[\mathbf{C}]_{p,q}$ stands for the element in the p -th row and q -th column of \mathbf{C} , $d_p, d_q \in \mathbb{L}$ are corresponding normalized antenna positions, and $c_0 = 1 > |c_1| > |c_2| > \dots > |c_B| > 0$. The mutual coupling effect can be neglected when the inter-element spacing is larger than $B\lambda/2$. Specifically, the mutual coupling coefficients are calculated by $c_s = c_1 e^{-j(s-1)/8} / s$ for $s \in \langle 1, B \rangle$ [17]. In this paper, unless otherwise indicated, we set $c_1 = 0.2e^{j\pi/3}$ and $B = 100$. In the presence of mutual coupling, the received signal model in (1) can be refined as

$$\tilde{\mathbf{x}}(l) = \mathbf{C}\mathbf{A}\mathbf{s}(l) + \mathbf{n}(l) \quad (8)$$

While the mutual coupling coefficients depend on the separations between sensors, we introduce a weight function [17] to better characterize the mutual coupling within a physical array. To this end, we first introduce the set $\mathbb{M}(s)$ composed of all the sensor pairs with separation of s , that is,

$$\mathbb{M}(s) = \{(n_1, n_2) | n_1 - n_2 = s; n_1, n_2 \in \mathbb{L}\} \quad (9)$$

Definition 3: For a physical array with location set \mathbb{L} , the weight function $w(s)$ is defined by [17]

$$w(s) = \text{Card}\{\mathbb{M}(s)\} \quad (10)$$

where $w(s)$ represents the number of sensor pairs with separation of s .

Definition 4: The coupling leakage of a physical array is defined as [17]

$$\gamma = \frac{\|\mathbf{C} - \text{diag}(\mathbf{C})\|_F}{\|\mathbf{C}\|_F} \quad (11)$$

C. Coprime Array With Displaced Subarrays

The CADiS proposed in [21] is composed of two displaced subarrays with N and $\tilde{M} - 1$ sensors. In this paper, we introduce the specified CADiS with $\tilde{M} = 2M$, where N and M are coprime integers with $M < N$, the total number of sensors is $T = N + 2M - 1$ and the displacement is H . The inter-element spacing of the subarray with N sensors is $M\lambda/2$ while that of the other subarray is $N\lambda/2$.

Since the newly introduced subarray, termed padded subarray, is composed of $\lfloor M/2 \rfloor$ sensors, we consider a tCADiS with $N + 2M - 1 - \lfloor M/2 \rfloor$ sensors in this part by removing the rightmost $\lfloor M/2 \rfloor$ sensors in the subarray with $2M - 1$ sensors

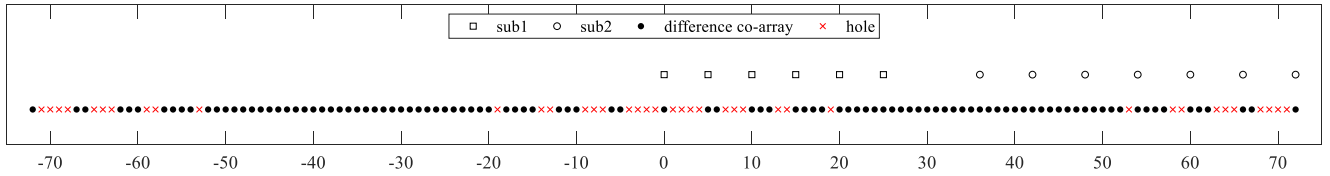


Fig. 1. An example of tCADiS configuration, where $N = 6$, $M = 5$, $T = 13$, and $H = 11$.

of the original CADiS. In this way, we can construct the PCA configuration with the total number of sensors $T = N + 2M - 1$, which is used for many coprime array configurations and is helpful for comparisons. Specifically, the location set of sensors in tCADiS is represented by

$$\mathbb{L}_{\text{tCADiS}} = \mathbb{L}_{\text{tCADiS}}^{(1)} \cup \mathbb{L}_{\text{tCADiS}}^{(2)} \quad (12)$$

where $\mathbb{L}_{\text{tCADiS}}^{(1)} = \{l_1 | l_1 = nM, n \in \langle 0, N-1 \rangle\}$ and $\mathbb{L}_{\text{tCADiS}}^{(2)} = \{l_2 | l_2 = mN + M(N-1) + (N+M), m \in \langle 0, 2M-2 - \lfloor M/2 \rfloor \rangle\}$, respectively, denote the location sets of the two subarrays.

In particular, it is proved in [21] that the displacement $H = N + M$ is the proper choice to produce the largest consecutive co-array of the original CADiS. Although this does not apply to tCADiS to generate a largest consecutive co-array, we found some other interesting merits of tCADiS with $H = N + M$, especially in terms of the hole locations in the difference co-array, which provide essential motivation for the proposed PCA configurations.

Property 1: The tCADiS with location set (12) possesses the following properties:

(a) The difference co-array has two consecutive co-arrays located at $\langle (M-1)(N-1), 2MN + M - 1 - \lfloor M/2 \rfloor N \rangle$ and $\langle -(2MN + M - 1 - \lfloor M/2 \rfloor N), -(M-1)(N-1) \rangle$.

(b) The tCADiS offers a total of $4MN + 2M - 1 - 2 \lfloor M/2 \rfloor N$ DOFs and $MN + 2M + N - 1 - \lfloor M/2 \rfloor N$ uniform DOFs.

(c) There exist holes in the cross-difference co-array located at $\pm[M(N-1) - (\tilde{a}M + \tilde{b}N) + (N+M)]$, where $\tilde{a} \geq 0$ and $\tilde{b} \geq 1$ are integers.

Because the tCADiS is directly constructed by simply removing the rightmost $\lfloor M/2 \rfloor$ sensors in CADiS, the proof of *Property 1*, which is omitted here, can be directly derived from the demonstrations of *Proposition 3.c* and *Proposition 4.b* in [21]. To illustrate this situation, we give an example of the tCADiS and the corresponding difference co-array in Fig. 1, where $N = 6$, $M = 5$, $T = 13$ and $H = 11$. It is explicitly seen that the difference co-array of tCADiS has two consecutive co-arrays located at $\langle 20, 52 \rangle$ and $\langle -52, -20 \rangle$ which are separated by holes located at $\{\pm 1, \pm 2, \pm 3, \pm 4, \pm 7, \pm 8, \pm 9, \pm 13, \pm 14, \pm 19\}$. As a result, the number of achievable uniform DOFs is 33 and only 16 signals can be detected at most when subspace algorithms based on the spatial smoothing technique or Toeplitz property are utilized [15]–[20], [22], [23]. In contrast, to utilize the total 105 DOFs provided by the difference co-array of tCADiS, sparse representation methods [21], [31]–[34] are required which suffer from high computational cost and complex combinatorial optimization.

D. Motivation

Intuitively, the consecutive co-arrays can be connected by filling the holes in the center of the difference co-array of tCADiS and then the number of uniform DOFs can be substantially increased. For the tCADiS illustrated in Fig. 1, a connected consecutive co-array located at $\langle -52, 52 \rangle$ can be obtained by adding a padded subarray with 10 physical sensors located at $\{1, 2, 3, 4, 7, 8, 9, 13, 14, 19\}$. An increased number of uniform DOFs of 105 can then be obtained, which is considerably attractive. However, the required number of filling sensors dramatically increases for a tCADiS with a large number of sensors. Moreover, the expression of the hole locations in CADiS, as given in [21], is not adequate to provide the exact location of the padded subarray. Besides, the number of sensor pairs with small separations increases due to the compact structure of the padded subarray, which results in severe mutual coupling.

III. HOLE REPRESENTATION APPROACHES AND PADDED COPRIME ARRAYS

In this section, we first provide the complete location expression of the holes in the difference co-array of tCADiS. Subsequently, we introduce two representation approaches which form the basis for the introduction of the proposed PCAs by incorporating the padded subarray with small number of sensors into the tCADiS. Finally, we propose a direct extension to the PCA configuration that allows a larger array aperture and an increase in the number of uniform DOFs.

A. Holes in the Difference Co-Array of tCADiS

While the location expression of holes provided by [21] only captures part of the holes in the difference co-array of CADiS, we generalize the *Proposition 3* and *4* in [21] and specify the complete location set \mathbb{H} of holes in the difference co-array of tCADiS by

$$\begin{cases} \mathbb{H} = \mathbb{H}_1 \cup \mathbb{H}_2 \cup \mathbb{H}_3 \cup \mathbb{H}_4 \\ \mathbb{H}_1 = \{h_1 | h_1 = MN - aM - bN\} \\ \quad \cap \langle 0, (N-1)(M-1) \rangle \\ \mathbb{H}_2 = \{h_2 | h_2 = I - h_1, h_1 \in \mathbb{H}_1\} \\ \mathbb{H}_3 = -\mathbb{H}_1 \\ \mathbb{H}_4 = -\mathbb{H}_2 \end{cases} \quad (13)$$

where $a \in \langle 1, N-2 \rangle$, $b \in \langle 1, M-1 \rangle$ and $I = M(N-1) + (M+N) + (2M-2 - \lfloor M/2 \rfloor)N$ is the physical array aperture. The proof, which is omitted here, is simple and follows the demonstration of *Proposition 3* in [21]. We note that

$\text{Card}\{\mathbb{H}_1\} = (M-1)(N-1)/2$ gives the number of physical sensors required in the padded subarray as the direct solution to fill the holes in the center of difference co-array and generate the connected consecutive co-array.

It can be concluded from (13) that the complete set of hole locations can be derived from \mathbb{H}_1 due to the symmetry property among the other subsets. As an example, for the tCADiS structure in Fig. 1, the complete set of holes in the difference co-array can be given by the union of $\mathbb{H}_1 = \{1, 2, 3, 4, 7, 8, 9, 13, 14, 19\}$, $\mathbb{H}_2 = \{53, 58, 59, 63, 64, 65, 68, 69, 70, 71\} = 72 - \mathbb{H}_1$, $\mathbb{H}_3 = \{-1, -2, -3, -4, -7, -8, -9, -13, -14, -19\} = -\mathbb{H}_1$ and $\mathbb{H}_4 = \{-53, -58, -59, -63, -64, -65, -68, -69, -70, -71\} = -\mathbb{H}_2 = \mathbb{H}_1 - 72$, where $I = 72$ is the array aperture.

B. Representation Approaches and PCAs

In this paper, we aim to lengthen the consecutive co-array of tCADiS by filling the holes in \mathbb{H}_1 and \mathbb{H}_3 , so that an augmented consecutive co-array can be obtained with increased uniform DOFs.

Theorem 1: (the first representation approach) For the tCADiS given by (12), the holes in the center of the difference co-array corresponding to the sets \mathbb{H}_1 and \mathbb{H}_3 in (13), can be generated from the differences between sensor locations in the subarray of tCADiS with location set $\langle 1, N-1 \rangle M$ and a padded subarray with location set $\mathbb{P}_1 = \{p_1 | p_1 = MN - b_1N, b_1 \in \langle 1, \lfloor M/2 \rfloor\}$.

Proof: Based on (13), we can start with the holes in \mathbb{H}_1 due to the symmetry property between \mathbb{H}_1 and \mathbb{H}_3 . Specifically, we introduce the first representation approach by characterizing the holes in \mathbb{H}_1 via $b \in \langle 1, M-1 \rangle$.

Let $b_1 \in \langle 1, \lfloor M/2 \rfloor \rangle$, then

$$\begin{aligned} h_1 &= MN - aM - b_1N \\ &= (MN - b_1N) - aM \end{aligned} \quad (14)$$

where $a \in \langle 1, N-2 \rangle$. Similarly, with $b_2 = (M - b_1) \in \langle M - \lfloor M/2 \rfloor, M-1 \rangle$, h_1 can be expressed as

$$\begin{aligned} h_1 &= MN - aM - b_2N \\ &= (N - a)M - (MN - b_1N) \end{aligned} \quad (15)$$

where $(N - a) \in \langle 2, N-1 \rangle$.

According to (14) and (15), it can be concluded that the holes for $b = b_1$ and $b = b_2$ in \mathbb{H}_1 and \mathbb{H}_3 can be interpreted as the differences between the sensor locations in the subarray of tCADiS and a missing sensor located at $MN - b_1N$. This follows by observing that the terms of aM in (14) and $(N - a)M$ in (15) can be regarded as the sensor locations in $\mathbb{L}_{\text{tCADiS}}^{(1)}$ of tCADiS ($a \in \langle 1, N-1 \rangle$). As a result, the holes in \mathbb{H}_1 and \mathbb{H}_3 can be classified into $\lfloor M/2 \rfloor$ groups via b . Furthermore, the padded subarray consisting of all the missing physical sensors, which result in the holes in the center of the difference co-array generated by tCADiS, has the location set $\mathbb{P}_1 = \{p_1 | p_1 = MN - b_1N, b_1 \in \langle 1, \lfloor M/2 \rfloor \rangle\}$. ■

Based on this representation, we propose a first type of PCA, named PCA-I, by incorporating the padded subarray \mathbb{P}_1 into

tCADiS. The location set $\mathbb{L}_{\text{PCA-I}}$ of sensors in PCA-I is specified by

$$\mathbb{L}_{\text{PCA-I}} = \mathbb{L}_{\text{tCADiS}} \cup \mathbb{P}_1 \quad (16)$$

where $\mathbb{L}_{\text{tCADiS}}$ is given by (12). The total number of sensors in PCA-I is $T = 2M + N - 1$ with N and M being coprime integers ($N > M \geq 2$).

Property 2: PCA-I with location set $\mathbb{L}_{\text{PCA-I}}$ defined by (16) possesses the following properties.

- PCA-I has a physical array aperture of $(3MN - N - \lfloor M/2 \rfloor N)$ and a difference co-array with a total number $5MN + M - (2 \lfloor M/2 \rfloor + 1)N$ of DOFs.
- The consecutive co-array in the difference co-array of PCA-I is located at $\langle -(2MN + M - 1 - \lfloor \frac{M}{2} \rfloor N), 2MN + M - 1 - \lfloor \frac{M}{2} \rfloor N \rangle$ and the number of uniform DOFs is $4MN + 2M - 2 \lfloor M/2 \rfloor N - 1$.
- The difference co-array of PCA-I only has holes located at its edges with location sets \mathbb{H}_2 and \mathbb{H}_4 .

An example of PCA-I is illustrated in Fig. 2 including the difference co-array, where $N = 6, M = 5, T = 15$ and $H = 11$. It is clearly seen that the holes in the center of the difference co-array of the tCADiS in Fig. 1 are accurately filled by adjoining the padded subarray $\mathbb{P}_1 = \{24, 18\}$ with only 2 sensors instead of 10 sensors in the direct padded subarray. Furthermore, a connected consecutive co-array located at $\langle -52, 52 \rangle$ is generated and an increased uniform DOF of 105 can be obtained, which is quite attractive.

According to (14) and (15), to fill the holes, only $N - 1$ sensors in subarray 1 of tCADiS, *i.e.*, with locations $\langle 1, N-1 \rangle M$, are needed while the subarray 1 has N sensors. As a result, we study the relation between the first $N - 1$ sensors with $\langle 0, N-2 \rangle M$ and the holes in \mathbb{H}_1 and \mathbb{H}_3 .

Theorem 2: (the second representation approach) For the tCADiS given by (12), the holes in the center of the difference co-array corresponding to \mathbb{H}_1 and \mathbb{H}_3 in (13), can be also generated from the differences between sensor locations in the subarray of tCADiS with location set $\langle 0, N-2 \rangle M$ and a padded subarray with $\mathbb{P}_2 = \{p_2 | p_2 = MN - b_1N - M, b_1 \in \langle 1, \lfloor M/2 \rfloor \rangle\}$.

Proof: In the second representation approach, we let $b = b_1 \in \langle 1, \lfloor M/2 \rfloor \rangle$ and rewrite h_1 as

$$\begin{aligned} h_1 &= MN - aM - b_1N \\ &= (MN - b_1N - M) - (a - 1)M \end{aligned} \quad (17)$$

where $(a - 1) \in \langle 0, N-3 \rangle$. Similarly, with $b_2 = (M - b_1) \in \langle M - \lfloor M/2 \rfloor, M-1 \rangle$, we can write

$$\begin{aligned} h_1 &= MN - aM - b_2N \\ &= (N - a - 1)M - (MN - b_1N - M) \end{aligned} \quad (18)$$

where $(N - a - 1) \in \langle 1, N-2 \rangle$.

According to (17) and (18), the holes for $b = b_1$ and $b = b_2$ are interpreted as the interaction between the subarray in tCADiS with location set $\langle 0, N-2 \rangle M$ and a missing physical sensor located at $MN - b_1N - M$. Resultantly, the padded subarray consisting of all the missing sensors needed to generate the holes in \mathbb{H}_1 and \mathbb{H}_3 , has the location set $\mathbb{P}_2 = \{p_2 | p_2 = MN - b_1N - M, b_1 \in \langle 1, \lfloor M/2 \rfloor \rangle\}$. ■

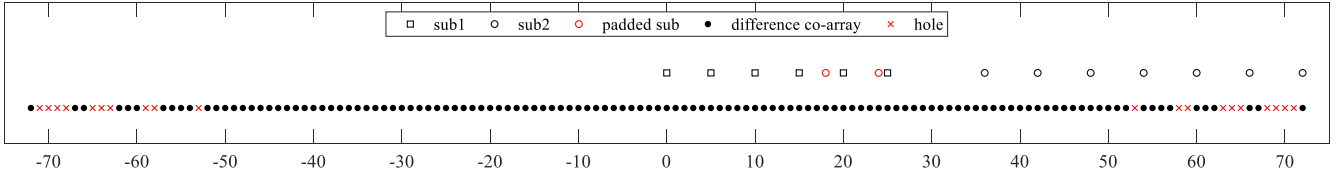


Fig. 2. An example of PCA-I, where $N = 6$, $M = 5$, $T = 15$, and $H = 11$.

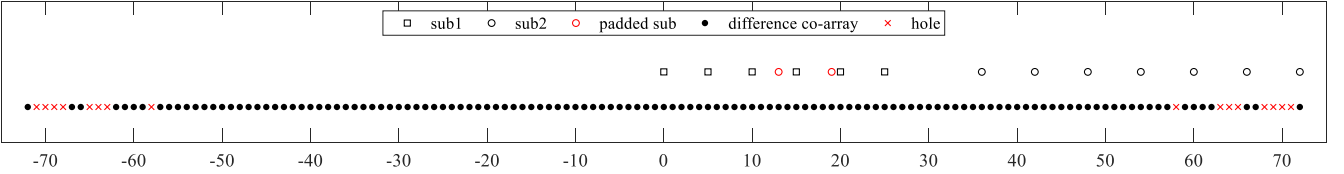


Fig. 3. An example of PCA-II, where $N = 6$, $M = 5$, $T = 15$, and $H = 11$.

Based on this alternative representation, we propose a second type of PCA, *i.e.*, PCA-II, by incorporating the padded subarray \mathbb{P}_2 into tCADiS. The location set $\mathbb{L}_{\text{PCA-II}}$ of sensors in PCA-II is specified by

$$\mathbb{L}_{\text{PCA-II}} = \mathbb{L}_{\text{tCADiS}} \cup \mathbb{P}_2 \quad (19)$$

The total number of sensors in PCA-II is $T = 2M + N - 1$, where N and M are coprime integers with $N > M \geq 3$.

Property 3: PCA-II with location set $\mathbb{L}_{\text{PCA-II}}$ defined by (19) possesses the following properties.

- PCA-II has a physical array aperture of $(3MN - N - \lfloor M/2 \rfloor N)$ and a difference co-array with a total number $5MN + 3M - (2 \lfloor M/2 \rfloor + 1)N - 2$ of DOFs.
- The consecutive co-array has the location set of $\langle -(2MN + 2M - 1 - \lfloor \frac{M}{2} \rfloor N), 2MN + 2M - 1 - \lfloor \frac{M}{2} \rfloor N \rangle$ and the number of uniform DOFs is $4MN + 4M - 2 \lfloor M/2 \rfloor N - 1$.
- The difference co-array of PCA-II has holes located at its edges with location sets \mathbb{H}_2 and \mathbb{H}_4 .

An example of PCA-II is shown Fig. 3, where $N = 6$, $M = 5$, $T = 15$ and $H = 11$. It can be explicitly seen that the holes at \mathbb{H}_1 and \mathbb{H}_3 in the difference co-array of tCADiS can be generated by adjoining the padded subarray $\mathbb{P}_2 = \{19, 13\}$ with only $\lfloor M/2 \rfloor = 2$ sensors. In particular, as compared with PCA-I in Fig. 2, the difference co-array of PCA-II has an augmented consecutive co-array located at $\langle -57, 57 \rangle$ with 115 uniform DOFs, compared to 105 for PCA-I. This further motivates the analysis of the interaction between the padded subarray and the subarray 2 in tCADiS.

Based on (13), we can express the hole locations in \mathbb{H}_2 by

$$\begin{aligned} h_2 &= I - h_1 \\ &= 2MN - N - \lfloor M/2 \rfloor N + aM + b_1N \\ &= [N(M+1) + (2M-2 - \lfloor M/2 \rfloor)N + (a-1)M] \\ &\quad - (MN - b_1N - M) \end{aligned} \quad (20)$$

where $I = N(M+1) + (2M-2 - \lfloor M/2 \rfloor)N$ represents the array aperture of tCADiS and $b_1 \in \langle 1, \lfloor M/2 \rfloor \rangle$. In the case $a =$

1, $[N(M+1) + (2M-2 - \lfloor M/2 \rfloor)N]$ gives the location of the rightmost sensor in tCADiS and $MN - b_1N - M$ gives the sensor locations in the padded subarray \mathbb{P}_2 . Consequently, the holes at the edge of the difference co-array for $a = 1$ can be filled, which explains the increased number of uniform DOFs of PCA-II as compared with PCA-I.

Remark 1: In fact, according to (14)-(15) and (17)-(18), two alternative sensors with location $MN - b_1N$ and $MN - M - b_1N$, respectively, are available to fill the holes in \mathbb{H}_1 and \mathbb{H}_3 corresponding to $b = b_1 \in \langle 1, \lfloor M/2 \rfloor \rangle$ and $b = (M - b_1)$. In turn, this implies that the location set of the padded subarray has $\lfloor \frac{M}{2} \rfloor^2$ solutions. To be specific, the proposed PCA-I and PCA-II are two special solutions. Besides, an augmented consecutive co-array as that of PCA-II can be generated when the padded subarray has a sensor located at $MN - M - b_1N$.

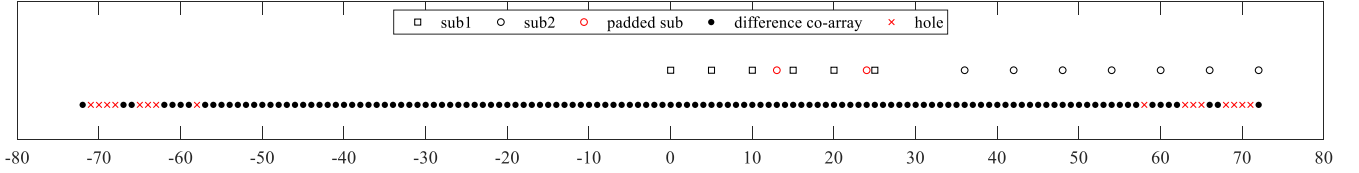
On the basis of *Remark 1*, we propose the third type of PCA, named PCA-III, which is obtained from another solution to the padded subarray. The location set $\mathbb{L}_{\text{PCA-III}}$ of sensors in PCA-III can be specified by

$$\mathbb{L}_{\text{PCA-III}} = \mathbb{L}_{\text{tCADiS}} \cup \mathbb{P}_3 \quad (21)$$

where $\mathbb{P}_3 = \mathbb{P}_{31} \cup \mathbb{P}_{32} = \{p_3 | p_3 = MN - b_1N, b_1 \in \langle 1, \lfloor M/2 \rfloor - 1 \rangle\} \cup \{MN - M - \lfloor M/2 \rfloor N\}$ gives the third solution to the location set of the padded subarray. The total number of sensors is $T = 2M + N - 1$, where N and M are coprime integers with $N > M \geq 3$. An example of PCA-III is shown in Fig. 4, where $N = 6$, $M = 5$, $T = 15$, $H = 11$ and the location set of the padded subarray is given by $\{24, 13\}$. It can be seen that, similar to PCA-II, the difference co-array of PCA-III possesses the augmented consecutive co-array located at $\langle -57, 57 \rangle$ and the increased number of uniform DOFs 115.

C. Extended PCA

In this part, based on PCA-III, we propose an extended PCA, termed ePCA, to obtain a further increase in the number of uniform DOFs and an enlarged array aperture compared with PCA-III.


 Fig. 4. An example of PCA-III, where $N = 6$, $M = 5$, $T = 15$, and $H = 11$.

According to *Proposition 3.c* in [21], extra holes with location sets $\mathbb{H}_5 = \{h_5 | h_5 = m_1 N + M, m_1 \in \langle 1, 2M - 1 - \lfloor M/2 \rfloor \rangle\}$ and $-\mathbb{H}_5$ will appear if we shift the subarray $\mathbb{L}_{\text{tCADiS}}^{(2)}$ in tCADiS to the right by M . The shift operation leads to the translation of the holes with location set $\mathbb{H}'_2 = \{h'_2 | h'_2 = (I - h_1) + M, h_1 \in \mathbb{H}_1\}$, which is not the objective in our work. Specifically, we calculate the difference between $p_3 \in \mathbb{P}_3$ and $MN - M - \lfloor M/2 \rfloor N \in \mathbb{P}_3$ in PCA-III as

$$\begin{aligned} p' &= p_3 - (MN - M - \lfloor M/2 \rfloor N) \\ &= (\lfloor M/2 \rfloor - b_1)N + M \end{aligned} \quad (22)$$

where $(\lfloor M/2 \rfloor - b_1) \in \langle 1, \lfloor M/2 \rfloor - 1 \rangle$. It can be seen from (22) that the padded subarray in PCA-III can produce some virtual sensors to fill the holes in \mathbb{H}_5 , which motivates us to make a similar shift by M of the subarray with location set $\mathbb{L}_{\text{tCADiS}}^{(2)}$ in PCA-III. Actually, the resulting ePCA leads to a further extension of the consecutive co-array and array aperture. Specifically, the location set \mathbb{L}_{ePCA} of sensors in ePCA is given as

$$\mathbb{L}_{\text{ePCA}} = \mathbb{L}_{\text{tCADiS}}^{(1)} \cup \mathbb{L}_{\text{tCADiS}}^{(2)} \cup \mathbb{P}_3 \quad (23)$$

where $\mathbb{L}_{\text{tCADiS}}^{(2)} = \{l_{21} | l_{21} = mN + M(N - 1) + (N + 2M), m \in \langle 0, 2M - 2 - \lfloor \frac{M}{2} \rfloor \rangle\}$, $\mathbb{L}_{\text{tCADiS}}^{(1)}$ is the location set of the subarray 1 in tCADiS and \mathbb{P}_3 is the padded subarray solution underlying PCA-III with $N > M \geq 4$.

Next, we provide more details about the hole filling in ePCA by directly extending PCA-III, where we only consider the non-negative part of the difference co-array for simplicity due to the symmetry property of hole locations. It can be observed that the potential holes caused by the shift operation are the result of the interaction between the subarray with location set $\mathbb{L}_{\text{tCADiS}}^{(2)}$ and the other two subarrays in PCA-III. For example, the holes with location sets \mathbb{H}_5 and \mathbb{H}'_2 are related to the subarray $\mathbb{L}_{\text{tCADiS}}^{(1)}$ and the shift operation of the subarray $\mathbb{L}_{\text{tCADiS}}^{(2)}$. Besides, the virtual sensors with locations in the difference co-array of PCA-III can likely become holes in the difference co-array of ePCA due to the shift operation. Specifically, for the subarrays with sensor location sets $\mathbb{L}_{\text{tCADiS}}^{(2)}$ and \mathbb{P}_3 , we have

$$\begin{cases} l_2 - p_{31} = (m + b_1 + 1)N \\ l_2 - p_{32} = (m + \lfloor M/2 \rfloor + 1)N + M \end{cases} \quad (24)$$

where $l_2 \in \mathbb{L}_{\text{tCADiS}}^{(2)}$, $p_{31}, p_{32} \in \mathbb{P}_3$, $(m + b_1 + 1) \in \langle 2, 2M - 2 \rangle$ and $(m + \lfloor M/2 \rfloor + 1) \in \langle \lfloor M/2 \rfloor + 1, 2M - 1 \rangle$. Recalling the definition of \mathbb{H}_5 , the complete set of holes due to

the shift operation can be represented by $\mathbb{H}_{\text{III}} = \mathbb{H}_{\text{III}}^{(1)} \cup \mathbb{H}_{\text{III}}^{(2)} = \{h_{\text{III}}^{(1)} | h_{\text{III}}^{(1)} = m_2 N, m_2 \in \langle 2, 2M - 2 \rangle\} \cup \{h_{\text{III}}^{(2)} | h_{\text{III}}^{(2)} = m_3 N + M, m_3 \in \langle 1, 2M - 1 \rangle\}$.

Subsequently, to characterize the hole filling in ePCA, we calculate the differences between locations of the sensors in subarrays $\mathbb{L}_{\text{tCADiS}}^{(2)}$ and \mathbb{P}_3 , *i.e.*:

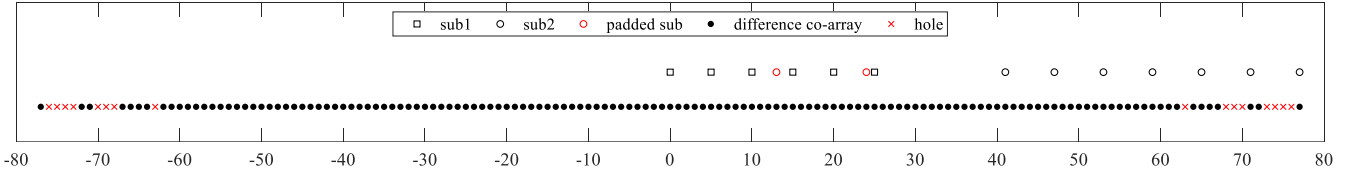
$$\begin{cases} l_{21} - p_{31} = (m + b_1 + m)N + M \\ l_{21} - p_{32} = (m + \lfloor M/2 \rfloor + 1)N + 2M \end{cases} \quad (25)$$

where $l_{21} \in \mathbb{L}_{\text{tCADiS}}^{(2)}$, $(m + b_1 + 1) \in \langle 2, 2M - 2 \rangle$ and $(m + \lfloor M/2 \rfloor + 1) \in \langle \lfloor M/2 \rfloor + 1, 2M - 1 \rangle$. Specifically, the holes in $\mathbb{H}_{\text{III}}^{(1)}$ can be partly filled by the subarray $\mathbb{L}_{\text{tCADiS}}^{(2)}$ which can yield the differences $\{m_4 N, m_4 \in \langle 0, 2M - 2 - \lfloor M/2 \rfloor \rangle\}$. For the remaining holes, we exploit the sensor with position M and the subarray $\mathbb{L}_{\text{tCADiS}}^{(2)}$, where the difference set $\{(m + M + 1)N, (m + M + 1) \in \langle M + 1, 3M - 1 - \lfloor M/2 \rfloor \rangle\}$ can be obtained and $2M - 2 - \lfloor M/2 \rfloor \geq (M + 1) - 1$, *i.e.*, $M \geq 3$, is required. Regarding the holes in $\mathbb{H}_{\text{III}}^{(2)}$, based on (22) and (25), we can only fill the holes with $\mathbb{H}_{\text{III}}^{(2')} = \{h_{\text{III}}^{(2')} | h_{\text{III}}^{(2')} = m'_3 N + M, m'_3 \in \langle 1, 2M - 2 \rangle\}$, where $\lfloor M/2 \rfloor - 1 \geq (2 - 1)$, *i.e.*, $M \geq 4$, is required. In particular, the position of the remaining hole $(2M - 1)N + M$ can be expressed as $(M - 2)N + (N - 1)M + (2M + N)$ which is the position of the $(M - 2)$ -th physical sensor in the subarray with location set $\mathbb{L}_{\text{tCADiS}}^{(2)}$ in ePCA. Finally, we summarize the properties of ePCA as follows.

Property 4: For ePCA with location set \mathbb{L}_{ePCA} , the following properties apply.

- ePCA has an array aperture of $(3MN - N - \lfloor M/2 \rfloor N + M)$ and a difference co-array with a total number $5MN + 3M - (2 \lfloor M/2 \rfloor + 1)N + 2 \lfloor M/2 \rfloor$ of DOFs.
- The consecutive co-array has the location set $\langle -(2MN + 3M - 1 - \lfloor \frac{M}{2} \rfloor)N, 2MN + 3M - 1 - \lfloor \frac{M}{2} \rfloor N \rangle$ and the number of uniform DOFs is $4MN + 6M - 2 \lfloor M/2 \rfloor N - 1$.
- The difference co-array of ePCA has holes located at $\mathbb{H}_e^+ = \{h_e | h_e = I_e - (MN - aM - bN)\}$ and $\mathbb{H}_e^- = -\mathbb{H}_e^+$, where $I_e = M(N - 1) + (2M + N) + (2M - 2 - \lfloor M/2 \rfloor)N$, $a \in \langle 2, N - 2 \rangle$ and $b \in \langle 1, M - 1 \rangle$.

An example of ePCA is presented in Fig. 5, including the physical array and the difference co-array, where $N = 6$, $M = 5$ and $T = 15$. According to Fig. 4 and Fig. 5, ePCA in this example can be obtained by shifting subarray 2 in PCA-III by $M = 5$ units to the right. As compared with PCA-II and PCA-III,

Fig. 5. An example of ePCA, where $N = 6$, $M = 5$, $T = 15$, and $H = 16$.TABLE I
CHARACTERISTICS OF DIFFERENT COPRIME ARRAY CONFIGURATIONS

	number of sensors	total DOF	uniform DOF
tCADiS	$2M + N - \lfloor M/2 \rfloor - 1$	$4MN + 2M - 1 - 2 \lfloor M/2 \rfloor N$	$MN + 2M + N - 1 - \lfloor M/2 \rfloor N$
CADiS [21]	$2M + N - 1$	$4MN + 2M - 1$	$MN + 2M + N - 1$
PCA-I	$2M + N - 1$	$5MN + M - (2 \lfloor M/2 \rfloor + 1)N$	$4MN + 2M - 2 \lfloor M/2 \rfloor N - 1$
PCA-II	$2M + N - 1$	$5MN + 3M - (2 \lfloor M/2 \rfloor + 1)N - 2$	$4MN + 4M - 2 \lfloor M/2 \rfloor N - 1$
ePCA	$2M + N - 1$	$5MN + 3M - (2 \lfloor M/2 \rfloor + 1)N + 2 \lfloor M/2 \rfloor$	$4MN + 6M - 2 \lfloor M/2 \rfloor N - 1$
ACA	$2M + N - 1$	$3MN + M - N$	$2MN + 2M - 1$
kECA	$kM + N - 1$	$(2k - 1)MN + M - N$	$2(k - 1)MN + 2M - 1$
CCA	$(k + 1)M + N - 2$	$2kMN - 2N + 1$	$2kMN - 2N + 1$
TCA	$M + N + \lfloor M/2 \rfloor - 1$	$3MN + M - N$	$2MN + 2M - 1$
SNA3	$N_1 + N_2$	$2N_2(N_1 + 1) - 1$	$2N_2(N_1 + 1) - 1$
ANA-I1	$N_1 + N_2$	$2N_2(N_1 + 1) + 2 \lceil (N_1 + 1)/2 \rceil - 1$	$2N_2(N_1 + 1) + 2 \lceil (N_1 + 1)/2 \rceil - 1$
ANA-I2	$N_1 + N_2$	$2N_2(N_1 + 1) + 2N_1 - 5$	$2N_2(N_1 + 1) + 2N_1 - 5$

TABLE II
OPTIMAL SOLUTION TO PCAS FOR MAXIMUM NUMBER OF UNIFORM DOFS

	PCA-I	PCA-II	ePCA
M even	$M = \frac{3T+5}{12}$	$M = \frac{3T+7}{12}$	$M = \frac{T+3}{4}$
M odd	$M = \frac{T+1}{4}$	$M = \frac{3T+5}{12}$	$M = \frac{3T+7}{12}$

ePCA can achieve a larger physical array aperture of 77 and generate an extended consecutive co-array located at $\langle -62, 62 \rangle$, which offers 10 additional uniform DOFs.

IV. DISCUSSION

A. Degree of Freedom

For comparison, we summarize the total number of DOFs and uniform DOFs (simplified as total DOF and uniform DOF) in Table I, respectively, of different coprime array configurations. We recall that CADiS [21] is composed of two subarrays with N and $2M - 1$ sensors, where the total number of sensors is $2M + N - 1$ and the displacement of the two subarrays is $N + M$. To obtain the maximum number of uniform DOFs, we calculate the optimal structure of PCAs, *i.e.*, PCA-I, PCA-II and ePCA, with a fixed number of sensors $T = 2M + N - 1$ by employing the Lagrange multiplier method as [23]. The optimal values,¹ of M are provided in Table II, while the final specifications of the optimal PCAs are obtained by maximizing the number of uniform DOFs in the case of odd and even M . It should be noted that the expressions for M in Table II

¹The results in Table II serve as initial guesses for the optimal selection of M , which will be refined with simple additional modifications, *i.e.* M and N are coprime integers and $M < N$.

are non-integers for most values of T and it is not simple to determine the final values of M and N with a fixed number of sensors T . In practice, we can first obtain the optimal non-integer result for M according to Table II and then consider the adjacent integers, taking into account required conditions on M and N , *i.e.*, $M < N$ and the coprimality relation. Finally, we can determine the desired specifications by calculating the uniform DOFs of each pair of M and N . For example, in the case $T = 30$ the optimal solution to PCA-I can be obtained as follows: From Table II, we have $\frac{T+1}{4} = 7.75$ for odd M and then M can take the values of $\{7, 9\}$ while $\frac{3T+5}{12} \approx 7.9$ for even M and the possible values are $\{6, 8\}$. Considering the requirements of $M < N$ and coprimality, the candidates (M, N) for PCA-I are $(6, 19)$, $(8, 15)$, $(7, 17)$ and $(9, 13)$. Finally, we calculate the uniform DOFs of the candidate specifications and the resulting optimal PCA-I is constructed with $M = 7$, $N = 17$ to obtain the maximum number of uniform DOFs.

In Table III, we compare the numbers of total number of DOFs and uniform DOFs for different coprime array configurations, all comprised of $T = 30$ sensors, and where each coprime array achieves the maximum number of uniform DOFs. While CADiS suffers from the holes in the center of its difference co-array, leading to the smallest number of uniform DOFs, the proposed PCAs can fill these holes, which results in a significant increase in the number of uniform DOFs. Compared with the CCA configuration [26] which has a difference co-array with hole-free property, both PCA-II and ePCA can obtain larger total number of DOFs and uniform DOFs, even with some holes at the end of the difference co-array. Besides, ePCA exhibits remarkable properties, being superior to the other coprime arrays in terms of both the total number of DOFs and uniform DOFs.

TABLE III
 COMPARISON OF SPARSE ARRAY CONFIGURATIONS WITH 30 SENSORS

	specified parameters	total DOF	uniform DOF
tCADiS	$M = 11, N = 14$	497	119
CADiS [21]	$M = 8, N = 15$	495	150
PCA-I	$M = 7, N = 17$	483	387
PCA-II	$M = 7, N = 17$	495	401
ePCA	$M = 9, N = 13$	503	417
TCA	$M = 11, N = 15$	491	351
ACA	$M = 8, N = 15$	353	255
kECA	$M = 4, N = 15, k = 4$	409	367
CCA	$M = 3, N = 14, k = 5$	393	393
SNA3	$N_1 = 15, N_2 = 15$	479	479
ANA-I1	$T = 30$	495	495
ANA-I2	$T = 30$	505	505

B. Mutual Coupling and Weight Function

In this part, we expose another advantage of the proposed PCAs over existing sparse array configurations, including the coprime and nested arrays, in that PCAs are less susceptible to mutual coupling. It is well-known that sensor pairs with small separations are the main cause of mutual coupling. In particular, the weights $w(1)$, $w(2)$ and $w(3)$ (see eq. (10)) have a major influence on the mutual coupling in a physical array [17].

Property 5: The PCAs, including PCA-I, PCA-II and ePCA, share the same weight function which is given by

$$w(s) = 1, \text{ if } M \text{ odd} \quad (26)$$

$$w(s) = \begin{cases} 1 & s \neq \frac{M}{2} \\ 2 & s = \frac{M}{2} \end{cases}, \text{ if } M \text{ even} \quad (27)$$

where $s \in \langle 1, M-1 \rangle$.

Proof: While the tCADiS allows the minimum inter-element spacing to be M ($M < N$) [21], we propose the PCAs by incorporating a padded subarray into tCADiS. As a result, the number of sensor pairs with separation of $\langle 1, M-1 \rangle$ depends on the interaction between the padded subarray and the subarray 1 in each PCA configuration. Here we only provide the detailed proof for PCA-I but the proofs for PCA-II and ePCA are similar. Assume that there are two sensor pairs generating the separation $s \in \langle 1, M-1 \rangle$, which can be represented by

$$\begin{aligned} |n_1 M - m_1 N| &= s \\ |n_2 M - m_2 N| &= s \end{aligned} \quad (28)$$

where $n_1, n_2 \in \langle 0, N-1 \rangle$ and $m_1, m_2 \in \langle 1, \lfloor \frac{M}{2} \rfloor \rangle$. We need to consider two cases.

1) If $n_1 M - m_1 N = s$ and $n_2 M - m_2 N = s$, we have

$$(n_1 - n_2)M = (m_1 - m_2)N \quad (29)$$

Due to the coprime property of M, N , the solution to (29) is $n_1 = n_2$ and $m_1 = m_2$, which means that only one sensor pair generates the separation s .

2) If $n_1 M - m_1 N = -s$ and $n_2 M - m_2 N = s$, we have

$$(n_1 + n_2)M = (m_1 + m_2)N \quad (30)$$

 TABLE IV
 FIRST THREE WEIGHT FUNCTIONS OF SPARSE ARRAY CONFIGURATIONS WITH 30 SENSORS

	specified parameters	$w(1)$	$w(2)$	$w(3)$	γ
tCADiS	$M = 11, N = 14$	0	0	0	0.0269
CADiS	$M = 8, N = 15$	0	0	0	0.0333
PCA-I	$M = 7, N = 17$	1	1	1	0.0752
PCA-II	$M = 7, N = 17$	1	1	1	0.0752
ePCA	$M = 9, N = 13$	1	1	1	0.0717
TCA	$M = 11, N = 15$	1	1	1	0.0704
ACA	$M = 8, N = 15$	2	2	2	0.0980
kECA	$M = 4, N = 15, k = 4$	2	2	2	0.1090
CCA	$M = 3, N = 14, k = 5$	4	3	14	0.1404
NA	$N_1 = 15, N_2 = 15$	15	14	13	0.2359
SNA3	$N_1 = 15, N_2 = 15$	1	7	2	0.1086
ANA-I1	$T = 30$	14	12	10	0.2207
ANA-I2	$T = 30$	2	13	2	0.1344

As $(n_1 + n_2) \in \langle 0, 2N-2 \rangle$, $(m_1 + m_2) \in \langle 2, 2 \lfloor \frac{M}{2} \rfloor \rangle$ and M, N are coprime integers, $n_1 + n_2 = N$ and $m_1 + m_2 = M$ are required. However, if M is an odd integer, $2 \lfloor \frac{M}{2} \rfloor = M-1 < M$ and $m_1 + m_2 < M$, where no solution exists. Besides, in the case of even M , since $m_1, m_2 \in \langle 1, \frac{M}{2} \rangle$ and $(m_1 + m_2) \in \langle 2, M \rangle$, $m_1 + m_2 = M$ and $m_1 = m_2 = M/2$, only two sensor pairs contribute to the separation s . Furthermore, if we assume $m_1 = m_2 = M/2$ in (28), we have $M(N - 2n_1) = 2s$. Since $2s \in \langle 2, 2M-2 \rangle$, s can only take the value of $M/2$ and $n_1 = (N-1)/2, n_2 = (N+1)/2$. Consequently, only two sensor pairs generate the separation $s = M/2$ if M is an even integer, while in other circumstances, $w(s) = 1$ with $s \in \langle 1, M-1 \rangle$, which proves the *Property 5*. ■

According to the weight function of PCAs given in (26) and (27), we conclude that the proposed PCAs can significantly reduce the mutual coupling due to the limited number of sensor pairs yielding small separations. Specifically, in Table IV, we list the values of the weight function $w(s)$ for $s = 1, 2$ and 3 , as well as the coupling leakage coefficient γ (11) for various types of array configurations, where the total number of sensors is $T = 30$. Note that two-level NA and SNA3 are composed of two subarrays with N_1 and N_2 sensors. It is clearly seen from this Table that CADiS achieves the smallest weight function values of 0 and coupling leakage of 0.0333, as it allows a large minimum inter-element spacing, which is considerably attractive. While CADiS benefits from the large total number of DOFs offered by the difference co-array, the holes in the center of the difference co-array significantly decrease the achievable number of uniform DOFs, which is seen from Table III. While the nested arrays have aroused considerable attention due to the hole-free property of their difference co-array, they exhibit larger values of the weight function and coupling leakage, which results in severe mutual coupling. On the contrary, the PCAs proposed here and the TCA from [24] can substantially limit the first three weight function values, $w(1) = w(2) = w(3) = 1$, while generating a large consecutive co-array to offer a competitive number of uniform DOFs. In this regard, we note from Table III that PCA-II and ePCA outperform the TCA and CADiS in terms

of both the total number of DOFs and uniform DOFs. In fact, the weight functions of PCA-I and PCA-II satisfy $w(s) = 1$ for all $s \in \langle 1, 6 \rangle$ while for ePCA, $w(s) = 1$ for all $s \in \langle 1, 8 \rangle$.

Remark 2: It follows from (26) and (27) that the first three values of the weight function, *i.e.*, $w(1)$, $w(2)$ and $w(3)$, of the proposed PCAs are independent of the number of sensors when $M > 4$. Specifically, in the case of $M = 4$, $w(1) = 1$, $w(2) = 2$ and $w(3) = 1$ while for all $M \geq 5$, $w(1) = w(2) = w(3) = 1$. In addition, although the first three weight values have a major effect on the mutual coupling, the proposed PCAs can limit the number of sensor pairs with separations of $\langle 1, M - 1 \rangle$, which is quite attractive to reduce the mutual coupling effect with large M .

Remark 3: It should be noted that TCA [24] is different from the proposed PCA configuration. Specifically, TCA was proposed by exploiting the redundancy in the difference co-array of the ACA in order to improve the number of DOFs with reduced mutual coupling, while the PCA configuration in this paper is constructed to fill the holes in the difference co-array of a tCADiS by carefully assembling a padded subarray. In particular, TCA can be regarded as a special case of PCA obtained by removing the rightmost $\lfloor M/2 \rfloor$ sensors in tCADiS and inserting a padded subarray located at $\langle 1, \lfloor M/2 \rfloor \rangle N$. In addition, it can be seen from Table III that the PCA configuration can obtain more uniform DOFs than TCA, while both PCA-II and ePCA can outperform TCA in terms of the total number of DOFs.

V. NUMERICAL SIMULATIONS

In this section, we conduct extensive simulations to validate the merits of the proposed PCAs over the coprime and nested array configurations in terms of DOA estimation performance and mutual coupling. In particular, the DOA estimation is achieved via the SS-ESPRIT algorithm [19] and its performance for the different array configurations is evaluated in terms of the root mean square error (RMSE) defined as,

$$\text{RMSE} = \sqrt{\frac{1}{1000K} \left(\sum_{q=1}^{1000} \sum_{k=1}^K (\theta_k - \hat{\theta}_{k,q})^2 \right)} \quad (31)$$

where θ_k represents the true DOA of the k -th signal in degrees and $\hat{\theta}_{k,q}$ denotes the corresponding estimate obtained with SS-ESPRIT at the q -trial. The simulation data is generated according to the physical model presented in Section II with parameter values as specified in Subsections B and C below. Various sparse array configurations are compared: in all cases, the total number of sensors is set to $T = 17$ while the other relevant parameters for the configurations under study are as listed in the second column of Table V. Besides, in the SS-ESPRIT algorithm (except in Subsection F), we decompose the consecutive co-array into $(p + 1)/2$ subarrays for each sparse array configuration under study to obtain the spatially smoothed matrix, where each subarray has $(p + 1)/2$ virtual sensors and p denotes the uniform DOF of each sparse array.

TABLE V
CHARACTERISTICS OF SPARSE ARRAY CONFIGURATIONS WITH 17 SENSORS

	specified parameters	total DOF	uniform DOF	γ
PCA-I	$M = 5, N = 8$	165	137	0.0986
PCA-II	$M = 5, N = 8$	173	147	0.0984
ePCA	$M = 5, N = 8$	179	157	0.0981
TCA	$M = 7, N = 8$	167	125	0.0950
k ECA	$M = 5, N = 8, k = 2$	117	89	0.1307
CCA	$M = 3, N = 10, k = 2$	101	101	0.1758
NA	$N_1 = 8, N_2 = 9$	161	161	0.2242
SNA3	$N_1 = 8, N_2 = 9$	161	161	0.1427
ANA-I1	$T = 17$	169	169	0.2156
ANA-I2	$T = 17$	173	173	0.1470
MRA	$T = 17$	187	187	0.1244

A. Parameters of Sparse Arrays

Table V compares the total number of DOFs, the number of uniform DOFs and the coupling leakage of the various sparse array configurations under study. Besides, Fig. 6 plots the corresponding weight functions of these configurations. The SNA and ANA configurations are generated as in [35], [36]. Moreover, k ECA in this case has the same configuration as ACA; hence we only provide the results of k ECA. The MRA configuration is obtained as in [37] and it is noteworthy that the structure of an advanced sparse array configuration, *i.e.*, MISC [38], is identical to that of MRA in the case of $T = 17$. Specifically, the sets of sensor locations for the all arrays under comparison are provided in Appendix A.

As seen from Table V, the proposed PCAs lead to a substantial increase of the uniform DOFs as compared with k ECA, CCA and TCA, even though the CCA has a hole-free difference co-array. While the nested arrays outperform the PCAs in terms of uniform DOF, ePCA achieves a larger value of total number of DOFs than the nested arrays. In particular, MRA can obtain the largest total and uniform DOFs. Furthermore, it can be seen in Fig. 6 that PCAs and TCA can remarkably limit the number of sensor pairs with small separations. Specifically, these configurations all achieve $w(1) = w(2) = w(3) = w(4) = 1$. On the contrary, the nested array configurations and MRA exhibit a larger number of sensor pairs with small separations, which explains their large coupling leakage, especially for NA and ANA-I1, as indicated by γ in Table V. As a result, the nested arrays and MRA are much more sensitive to mutual coupling than the proposed PCAs.

B. Grating Lobes of Different Array Structures

According to related works [39], [40], the peak sidelobe level (PSL) is typically employed to evaluate the capability of suppressing the grating lobes in sparse array design. Generally, a larger inter-element spacing will have an adverse effect on the grating lobes suppression. In this part, we provide the beam patterns of the physical arrays in Fig. 6, including the ULA with inter-element spacing of $\lambda/2$, CADiS [21], the proposed PCAs (ePCA and PCA-II), TCA [24], CCA [26], SNA3 [18],

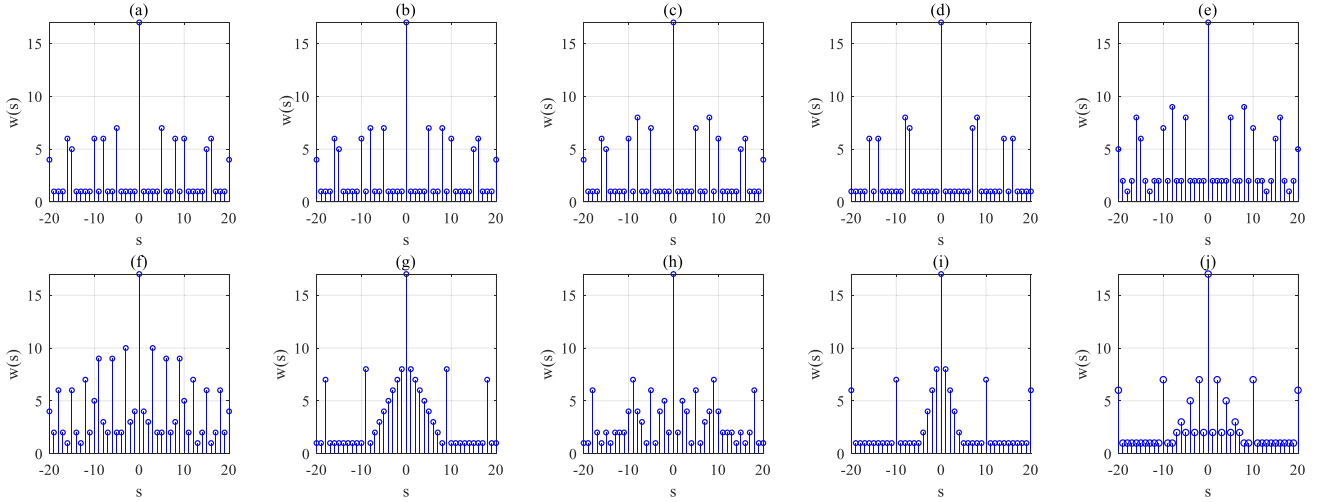


Fig. 6. Weight functions of the different sparse arrays under study with $T = 17$ sensors. (a) ePCA. (b) PCA-I. (c) PCA-II. (d) TCA. (e) k ECA. (f) CCA. (g) two-level NA. (h) SNA3. (i) ANA-I1. (j) ANA-I2.

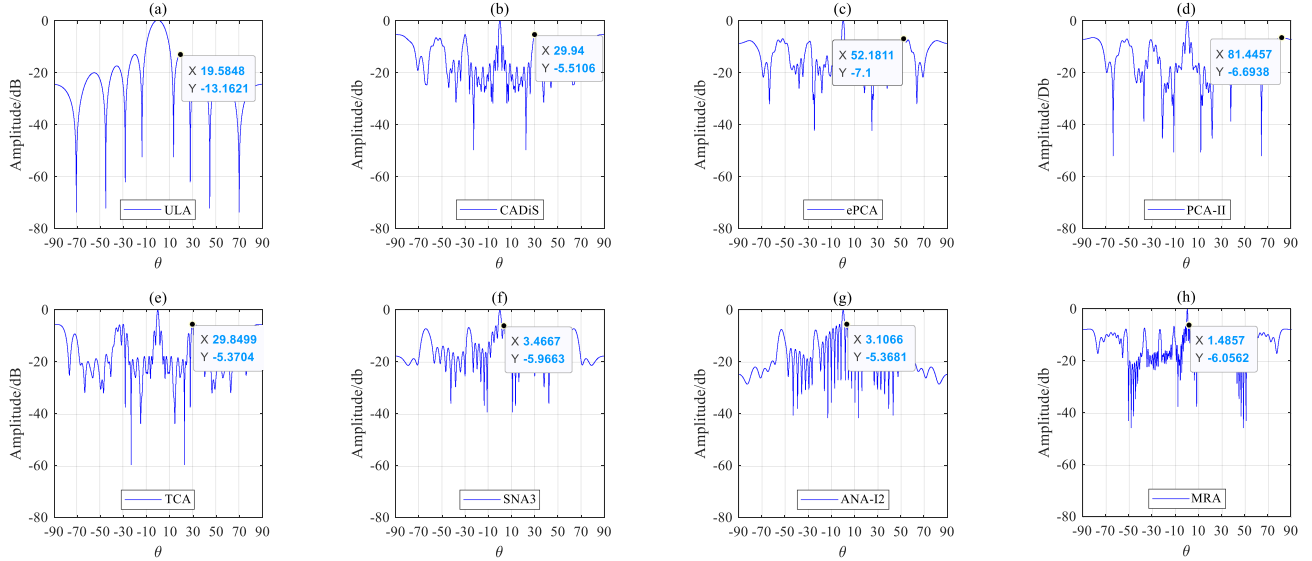


Fig. 7. Beam patterns of the different array structures under study with $T = 17$ sensors. (a) ULA. (b) CADiS. (c) ePCA. (d) PCA-II. (e) TCA. (f) SNA3. (g) ANA-I2. (h) MRA.

ANA-I2 [19] and MRA [37], where the total number of sensors is 17 and the sensor locations sets are provided as in Appendix A. It can be seen that ULA can obtain the lowest value of PSL (*i.e.*, -13.2 dB) while in particular, the proposed ePCA can achieve the lowest value of PSL (*i.e.*, -7.1 dB) among all the sparse arrays. In contrast, sparse arrays can generate much narrower main lobes than ULA since the sparse arrays have an extended array aperture.

C. DOA Estimation in the Absence of Mutual Coupling

Herein, we provide the simulated RMSE results of the array configurations listed in Table V in the absence of mutual coupling, where $K = 25$ signals impinge on the array from angles $\theta_k = -60 + 120(k - 1)/24$ ($k \in \langle 1, 25 \rangle$) and the

mutual coupling matrix is an identity matrix. Specifically, Fig. 8 depicts the RMSE results versus SNR, when the number of snapshots is set to $L = 1000$. It is clearly seen that the PCAs achieve smaller RMSE values than k ECA, CCA and TCA. Furthermore, ePCA can obtain more accurate DOA estimates than PCA-I and PCA-II, which verifies the effectiveness of the underlying extension concept. However, since the nested arrays have hole-free difference co-arrays with significant increase of uniform DOFs, their DOA estimation performance exceeds that of the proposed PCAs in the absence of mutual coupling. In addition, the RMSE results versus the number of snapshot L are given in Fig. 9, where $\text{SNR} = 0$ dB. It is observed that in all cases, the RMSE decreases as L increases and that ePCA performs the best among the coprime arrays in DOA estimation accuracy.

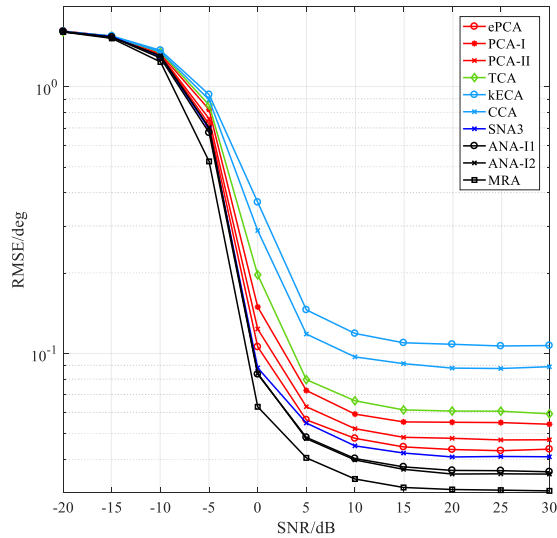


Fig. 8. RMSE versus SNR in the absence of mutual coupling, where $K = 25$, $L = 1000$.

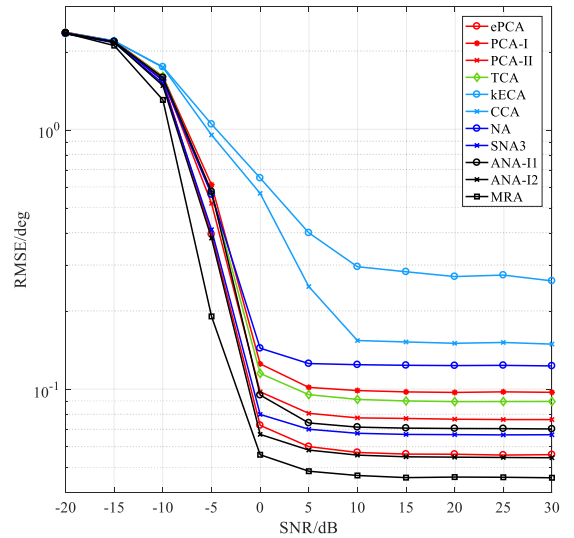


Fig. 10. RMSE versus SNR in the presence of mutual coupling, where $K = 17$, $L = 1500$.

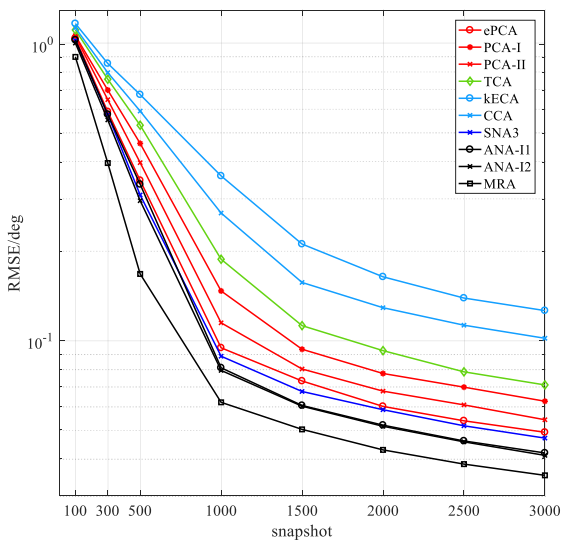


Fig. 9. RMSE versus number of snapshots L in the absence of mutual coupling, where $K = 25$, $\text{SNR} = 0\text{dB}$.

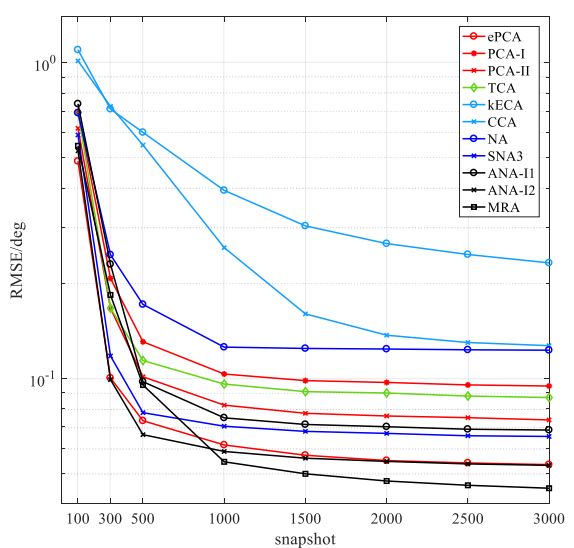


Fig. 11. RMSE versus number of snapshots L in the presence of mutual coupling, where $K = 17$, $\text{SNR} = 10\text{dB}$.

D. DOA Estimation in the Presence of Mutual Coupling

In this simulation, we compare the RMSE results of the various array configuration under study in the presence of mutual coupling, where in (7) $c_1 = 0.2e^{j\pi/3}$ and $B = 100$. The received signal is modeled as (8) and the array response is CA. The simulated scenario involves $K = 17$ signals with arrival angles $\theta_k = -60 + 120(k-1)/16$ ($k \in \langle 1, 17 \rangle$), while the number of snapshots is set to $L = 1500$. Specifically, the RMSE results versus SNR are plotted in Fig. 10 for the various array configurations under comparison. It is observed that the proposed PCAs can achieve fine DOA estimation performance. In particular, ePCA can obtain more accurate DOA estimates than the other array configurations, except ANA-I2 which has a considerably larger consecutive co-array than ePCA. Despite

having larger consecutive co-arrays, SNA3 and ANA-I1 cannot achieve as good performance as ePCA at high SNR due to the more severe effects of mutual coupling. Besides, we present the RMSE results versus the number of snapshot L in Fig. 11, where $\text{SNR} = 10\text{dB}$. It can be seen that ePCA can remarkably mitigate the mutual coupling effect and hence achieve a similar DOA estimation performance as ANA-I2 in the case of large number of snapshots.

In addition, we provide the RMSE results versus the amplitude of c_1 , i.e., $|c_1|$, in Fig. 12, where $\text{SNR} = 0\text{dB}$, other conditions being identical to those of Fig. 10. As nested arrays are attractive in offering a large number of uniform DOFs, they can provide accurate DOA estimates in the case of small $|c_1|$. Especially, MRA exhibits the best DOA estimation performance when

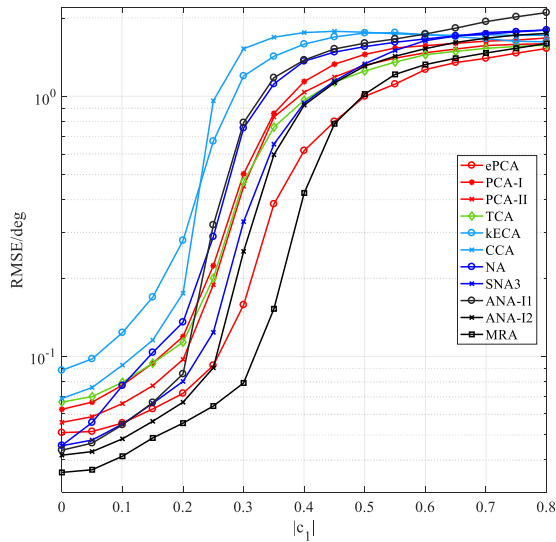


Fig. 12. RMSE versus $|c_1|$, where $B = 100$, $K = 17$, $\text{SNR} = 0\text{dB}$, and $L = 1500$.

$|c_1| \leq 0.45$. However, the sensor locations in the MRA are not available in closed-form and must therefore be calculated through a time-consuming search. Besides, ANA-12 can obtain more accurate DOA estimates than the proposed PCAs in the case of $|c_1| < 0.25$, but the nested arrays suffer from severe mutual coupling effect and offer drastically degraded DOA estimates with the increase of $|c_1|$ due to large number of sensor pairs with small separations. We note that when $|c_1| > 0.65$, $k\text{ECA}$ which has the smallest number of uniform DOFs, performs better in DOA estimation than the nested arrays. This further verifies that coprime arrays are of great interest in reducing mutual coupling. Finally, it is observed that the proposed ePCA is superior to other sparse arrays in the case of $|c_1| > 0.45$. In effect, ePCA can substantially increase the number of uniform DOFs by enlarging the consecutive co-array while reducing the effect of the mutual coupling by limiting the number of sensor pairs with small spacing. Finally, we note that a similar trend as in Fig. 12 is observed when the smaller value $B = 10$ is employed, other conditions being unchanged.

E. DOA Estimation With Randomly Distributed Signals

In this part, we provide the simulation results of DOA estimation with randomly distributed signals, where $\theta_k = -60 + 120\varepsilon_k$ and ε_k is a variable following the uniform distribution $U(0, 1)$. In Fig. 13, we calculate the RMSEs of the array configurations with randomly distributed signals in the absence of mutual coupling, where $K = 25$ and $L = 1500$. When $K = 25$ if the DOAs are randomly generated, it is inevitable that some of the sources will be closely located in the angular domain. Hence, the SS-ESPRIT algorithm will fail to distinguish some signals for some of the simulation trials, especially under the conditions of low SNR and small number of snapshots, which will get worse when DOA clustering arises. As a result, the RMSE curves in Fig. 13 are not as smooth as Fig. 8. However, it still can be seen from Fig. 13 that the nested arrays can obtain

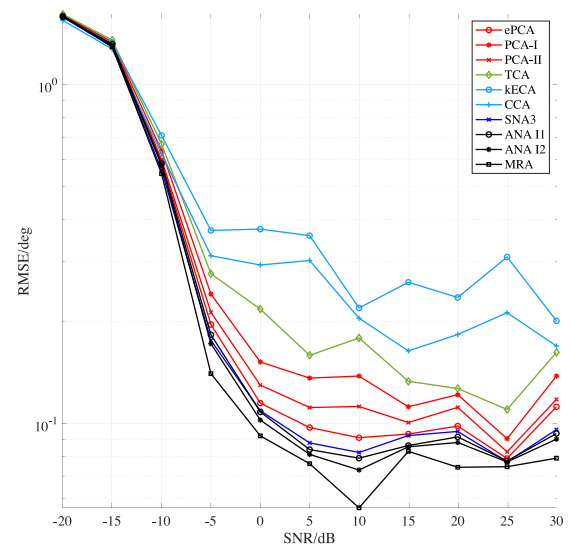


Fig. 13. RMSE with randomly distributed signals versus SNR in the absence of mutual coupling, where $K = 25$, $L = 1500$.

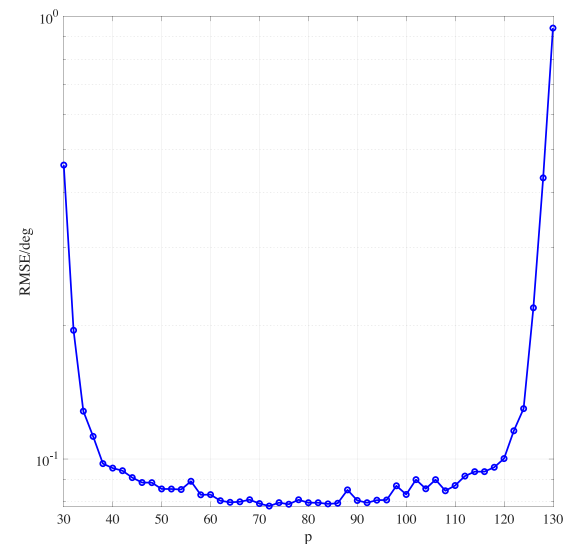


Fig. 14. RMSE versus the number of subarrays used for the spatially smoothed matrix of SS-ESPRIT with ePCA in the absence of mutual coupling, where $\text{SNR} = 0\text{dB}$ and $L = 1000$.

better DOA estimates than coprime arrays while the proposed ePCA is superior to the other coprime arrays.

F. Different Numbers of Subarrays Used for DOA Estimation

In this part, we provide the simulation results for DOA estimation performance with different numbers of subarrays used for the spatially smoothed matrix [15] of SS-ESPRIT, where the 17-element ePCA is used, $\text{SNR} = 0\text{dB}$, $L = 1000$ and $\theta_k = -60 + 120(k-1)/24$ ($k \in \langle 1, 25 \rangle$). It can be seen from the RMSE results in Fig. 14 that the DOA estimation performance approximately remains the same when the number of subarrays ranges from 70 to 86. In particular, according to [15], the number of subarrays essentially determines the number of

elements for each subarray which is the effective array size and gives the number of recognized sources. As a result, we usually decompose the consecutive co-array into $(p + 1)/2$ subarrays to identify up to $(p + 1)/2 - 1$ sources [15], [17]–[20], [23], [24], [26].

VI. CONCLUSION

In this work, we first provided a complete characterization for the hole locations in the difference co-array generated by tCADiS as the union of four subsets of locations related via simple symmetry properties. We then proposed two novel PCAs, termed as PCA-I and PCA-II, by incorporating the padded subarray into tCADiS to lengthen the consecutive segments in the difference co-array based on two representation approaches for the hole locations. Our approach not only contributes to increase the number of achievable uniform DOFs, but also helps reducing the mutual coupling by limiting the number of sensor pairs with small separations. In particular, ePCA, as an extension of the above PCA configurations, can provide a further increase in the number of uniform DOFs. Finally, numerical simulation results were provided to validate the theoretical findings and demonstrate the superiority of the proposed PCAs over existing coprime and nested arrays in terms of DOF, mutual coupling and DOA estimation accuracy.

APPENDIX A

The location sets of the arrays under study are given by

$$\mathbb{L}_{\text{ULA}} = \{0, 1, 2, 3, 4, 5, 6, 7, 8, 9, 10, 11, 12, 13, 14, 15, 16\}$$

$$\mathbb{L}_{\text{ePCA}} = \{0, 5, 10, 15, 19, 20, 25, 30, 32, 35, 53, 61, 69, 77, 85, 93, 101\}$$

$$\mathbb{L}_{\text{PCA-I}} = \{0, 5, 10, 15, 20, 24, 25, 30, 32, 35, 48, 56, 64, 72, 80, 88, 96\}$$

$$\mathbb{L}_{\text{PCA-II}} = \{0, 5, 10, 15, 19, 20, 25, 27, 30, 35, 48, 56, 64, 72, 80, 88, 96\}$$

$$\mathbb{L}_{\text{TCA}} = \{0, 7, 8, 14, 16, 21, 24, 28, 35, 42, 49, 64, 72, 80, 88, 96, 104\}$$

$$\mathbb{L}_{\text{KECA}} = \{0, 5, 8, 10, 15, 16, 20, 24, 25, 30, 32, 35, 40, 48, 56, 64, 72\}$$

$$\mathbb{L}_{\text{CCA}} = \{0, 3, 6, 9, 10, 12, 15, 18, 20, 21, 24, 27, 30, 40, 48, 49, 50\}$$

$$\mathbb{L}_{\text{SNA3}} = \{1, 3, 5, 6, 8, 11, 13, 16, 18, 27, 36, 45, 54, 63, 72, 80, 81\}$$

$$\mathbb{L}_{\text{ANA-II}} = \{1, 2, 3, 4, 10, 20, 30, 40, 50, 60, 70, 80, 81, 82, 83, 84, 85\}$$

$$\mathbb{L}_{\text{ANA-I2}} = \{1, 2, 4, 6, 8, 10, 20, 30, 40, 50, 60, 70, 80, 81, 83, 85, 87\}$$

$$\mathbb{L}_{\text{MRA}} = \{0, 1, 8, 18, 28, 38, 48, 58, 68, 78, 80, 82, 84, 87, 89, 91, 93\}$$

REFERENCES

- [1] J. Yu and C. Yeh, "Generalized eigenspace-based beamformers," *IEEE Trans. Signal Process.*, vol. 43, no. 11, pp. 2453–2461, Nov. 1995.
- [2] R. Lorenz and S. Boyd, "Robust minimum variance beamforming," *IEEE Trans. Signal Process.*, vol. 53, no. 5, pp. 1684–1696, May 2005.
- [3] S. Nai, W. Ser, Z. Yu, and H. Chen, "Iterative robust minimum variance beamforming," *IEEE Trans. Signal Process.*, vol. 59, no. 4, pp. 1601–1611, Apr. 2011.
- [4] R. Schmidt, "Multiple emitter location and signal parameter estimation," *IEEE Trans. Antennas Propag.*, vol. AP-34, no. 3, pp. 276–280, Mar. 1986.
- [5] R. Roy and T. Kailath, "ESPRIT-estimation of signal parameters via rotational invariance techniques," *IEEE Trans. Acoust. Speech Signal Process.*, vol. 37, no. 7, pp. 984–995, Jul. 1989.
- [6] C. Zhou, Y. Gu, S. He, and Z. Shi, "A robust and efficient algorithm for coprime array adaptive beamforming," *IEEE Trans. Veh. Technol.*, vol. 67, no. 2, pp. 1099–1112, Feb. 2018.
- [7] H. Krim and M. Viberg, "Two decades of array signal processing research: The parametric approach," *IEEE Signal Process. Mag.*, vol. 13, no. 4, pp. 67–94, Jul. 1996.
- [8] L. Godara, "Application of antenna arrays to mobile communications, part II: Beam-forming and direction-of-arrival considerations," *Proc. IEEE*, vol. 85, no. 8, pp. 1195–1245, Aug. 1997.
- [9] S. H. Talisa, K. W. O'Haver, T. M. Comberiate, M. D. Sharp, and O. F. Somerlock, "Benefits of digital phased array radars," *Proc. IEEE*, vol. 104, no. 3, pp. 530–543, Mar. 2016.
- [10] X. Zhang, X. Gao, and D. Xu, "Novel blind carrier frequency offset estimation for OFDM system with multiple antennas," *IEEE Trans. Wireless Commun.*, vol. 9, no. 3, pp. 881–885, Mar. 2010.
- [11] Z. Ye, J. Dai, X. Xu, and X. Wu, "DOA estimation for uniform linear array with mutual coupling," *IEEE Trans. Aerosp. Electron. Syst.*, vol. 45, no. 1, pp. 280–288, Jan. 2009.
- [12] J. Dai, D. Zhao, and X. Ji, "A sparse representation method for DOA estimation with unknown mutual coupling," *IEEE Antennas Wireless Propag. Lett.*, vol. 11, no. 1, pp. 1210–1213, 2012.
- [13] B. Liao, Z. Zhang, and S. Chan, "DOA estimation and tracking of ULAs with mutual coupling," *IEEE Trans. Aerosp. Electron. Syst.*, vol. 48, no. 1, pp. 891–905, Jan. 2012.
- [14] A. Moffet, "Minimum-redundancy linear arrays," *IEEE Trans. Antennas Propag.*, vol. AP-16, no. 2, pp. 172–175, Mar. 1968.
- [15] P. Pal and P. Vaidyanathan, "Nested arrays: A novel approach to array processing with enhanced degrees of freedom," *IEEE Trans. Signal Process.*, vol. 58, no. 8, pp. 4167–4181, Aug. 2010.
- [16] P. Vaidyanathan and P. Pal, "Sparse sensing with co-prime samplers and arrays," *IEEE Trans. Signal Process.*, vol. 59, no. 2, pp. 573–586, Feb. 2011.
- [17] C. Liu and P. Vaidyanathan, "Super nested arrays: Linear sparse arrays with reduced mutual coupling—Part I: Fundamentals," *IEEE Trans. Signal Process.*, vol. 64, no. 15, pp. 3997–4012, Aug. 2016.
- [18] C. Liu and P. Vaidyanathan, "Super nested arrays: Linear sparse arrays with reduced mutual coupling—Part II: High-order extensions," *IEEE Trans. Signal Process.*, vol. 64, no. 16, pp. 4203–4217, Aug. 2016.
- [19] J. Liu, Y. Zhang, Y. Lu, S. Ren, and S. Cao, "Augmented nested arrays with enhanced DOF and reduced mutual coupling," *IEEE Trans. Signal Process.*, vol. 65, no. 21, pp. 5549–5563, Nov. 2017.
- [20] P. Pal and P. Vaidyanathan, "Coprime sampling and the MUSIC algorithm," in *Proc. IEEE Digit. Signal Process. Workshop/IEEE Signal Process. Edu. Workshop*, Sedona, AZ, USA, Jan. 2011, pp. 289–294.
- [21] S. Qin, Y. Zhang, and M. Amin, "Generalized coprime array configurations for direction-of-arrival estimation," *IEEE Trans. Signal Process.*, vol. 63, no. 6, pp. 1377–1390, Mar. 2015.

- [22] C. Liu and P. Vaidyanathan, "Remarks on the spatial smoothing step in coarray MUSIC," *IEEE Signal Process. Lett.*, vol. 22, no. 9, pp. 1438–1442, Sep. 2015.
- [23] W. Zheng, X. Zhang, and J. Shi, "Sparse extension array geometry for DOA estimation with nested MIMO radar," *IEEE Access*, vol. 5, pp. 9580–9586, 2017.
- [24] A. Raza, W. Liu, and Q. Shen, "Thinned coprime array for second-order difference co-array generation with reduced mutual coupling," *IEEE Trans. Signal Process.*, vol. 67, no. 8, pp. 2052–2065, Apr. 2019.
- [25] W. Wang, S. Ren, and Z. Chen, "Unified coprime array with multi-period subarrays for direction-of-arrival estimation," *Digit. Signal Process.*, vol. 74, pp. 30–42, 2018.
- [26] X. Wang and X. Wang, "Hole identification and filling in k -times extended co-prime arrays for highly-efficient DOA estimation," *IEEE Trans. Signal Process.*, vol. 67, no. 10, pp. 2693–2706, May 2019.
- [27] B. Friedlander and A. J. Weiss, "Direction finding in the presence of mutual coupling," *IEEE Trans. Antennas Propag.*, vol. 39, no. 3, pp. 273–284, Mar. 1991.
- [28] T. Svantesson, "Modeling and estimation of mutual coupling in a uniform linear array of dipoles," in *Proc. IEEE Int. Conf. Acoust., Speech, Signal Process.*, Phoenix, AZ, USA, Mar. 1999, pp. 2961–2964.
- [29] T. Svantesson, "Mutual coupling compensation using subspace fitting," in *Proc. IEEE Sensor Array Multichannel Signal Process. Workshop*, Cambridge, MA, USA, Mar. 2000, pp. 494–498.
- [30] F. Sellone and A. Serra, "A novel online mutual coupling compensation algorithm for uniform and linear arrays," *IEEE Trans. Signal Process.*, vol. 55, no. 2, pp. 560–573, Feb. 2007.
- [31] C. Zhou, Y. Gu, X. Fan, Z. Shi, G. Mao, and Y. D. Zhang, "Direction-of-arrival estimation for coprime array via virtual array interpolation," *IEEE Trans. Signal Process.*, vol. 66, no. 22, pp. 5956–5971, Nov. 2018.
- [32] D. Malioutov, M. Cetin, and A. Willsky, "A sparse signal reconstruction perspective for source localization with sensor arrays," *IEEE Trans. Signal Process.*, vol. 53, no. 8, pp. 3010–3022, Aug. 2005.
- [33] Z. Shi, C. Zhou, Y. Gu, N. A. Goodman, and F. Qu, "Source estimation using coprime array: A sparse reconstruction perspective," *IEEE Sensors J.*, vol. 17, no. 3, pp. 755–765, Feb. 2017.
- [34] J. Shi, G. Hu, X. Zhang, F. Sun, and H. Zhou, "Sparsity-based two-dimensional DOA estimation for coprime array: From sum-difference coarray viewpoint," *IEEE Trans. Signal Process.*, vol. 65, no. 21, pp. 5591–5604, Nov. 2017.
- [35] C. Liu, "Super nested arrays (1D)," Aug. 2016. [Online]. Available: <https://systems.caltech.edu/dsp/students/elliou/SuperNested.html>
- [36] J. Liu, "Augmented nested arrays," Jul. 2017. [Online]. Available: <https://www.mathworks.com/matlabcentral/fileexchange/57648-augmented-nested-array>
- [37] M. Ishiguro, "Minimum redundancy linear arrays for a large number of antennas," *Radio Sci.*, vol. 15, no. 6, pp. 1163–1170, 1980.
- [38] Z. Zheng, W.-Q. Wang, Y. Kong, and Y. D. Zhang, "MISC array: A new sparse array design achieving increased degrees of freedom and reduced mutual coupling effect," *IEEE Trans. Signal Process.*, vol. 67, no. 7, pp. 1728–1741, Apr. 2019.
- [39] L. Cen, W. Ser, Z. Yu, S. Rahardja, and W. Cen, "Linear sparse array synthesis with minimum number of sensors," *IEEE Trans. Antennas Propag.*, vol. 58, no. 3, pp. 720–726, Mar. 2009.
- [40] X. Zhao, Q. Yang, and Y. Zhang, "Compressed sensing approach for pattern synthesis of maximally sparse non-uniform linear array," *IET Microw., Antennas Propag.*, vol. 8, no. 5, pp. 301–307, 2013.